Acta Crystallographica Section F
Structural Biology and Crystallization Communications
ISSN 1744-3091

Crystallization and preliminary characterization of a novel haem-binding protein of *Streptomyces reticuli*

Peijian Zou,[a,b] Matthew R. Groves,[a] Sandra D. Viale-Bouroncle[c] and Darío Ortiz de Orué Lucana[c]*

[a]EMBL Outstation Hamburg, c/o DESY, Notkestrasse 85, 22607 Hamburg, Germany, [b]Institute of Structural Biology, Helmholtz Zentrum München, Ingolstädter Landstrasse 1, 85764 Neuherberg, Germany, and [c]Universität Osnabrück, FB Biologie/Chemie, Angewandte Genetik der Mikroorganismen, Barbarastrasse 13, 49069 Osnabrück, Germany

Correspondence e-mail: ortiz@biologie.uni-osnabrueck.de

Received 18 February 2008
Accepted 27 March 2008

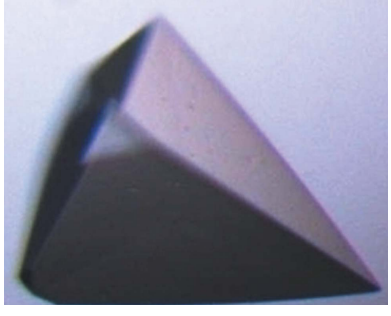

Streptomyces reticuli is a soil-growing Gram-positive bacteria that has been shown to secrete a novel haem-binding protein known as HbpS. Sequence analysis reveals that homologues of HbpS are found in a wide variety of bacteria, including different Actinobacteria and the Gram-negative *Vibrio cholera* and *Klebsiella pneumoniae*. The *in vivo* production of HbpS is greatly increased when *S. reticuli* is cultured in the presence of the natural antibiotic haemin (Fe^{3+} oxidized form of haem). Mutational analysis demonstrated that HbpS significantly increases the resistance of *S. reticuli* to toxic concentrations of haemin. Previous data show that the presence of the newly identified two-component sensor system SenS–SenR also considerably enhances the resistance of *S. reticuli* to haemin and the redox-cycling compound plumbagin, suggesting a role in the sensing of redox changes. Specific interaction between HbpS and SenS–SenR, which regulates the expression of the catalase–peroxidase CpeB, as well as HbpS, has been demonstrated *in vitro*. HbpS has been recombinantly overexpressed, purified and crystallized in space group $P2_13$, with a cell edge of 152.5 Å. Diffraction data were recorded to a maximal resolution of 2.25 Å and phases were obtained using the SAD method from crystals briefly soaked in high concentrations of sodium bromide.

1. Introduction

Streptomyces is the largest genus of Actinobacteria, with more than 500 species currently documented. The species are found worldwide and are characterized by a complex developmental life cycle and secondary metabolism. Indeed, *Streptomyces* spp. produce over two-thirds of naturally occurring antibiotics (*e.g.* neomycin and chloramphenicol). The Gram-positive soil bacterium *S. reticuli* has recently been shown to produce an extracellularly located novel haem-binding protein named HbpS (Ortiz de Orué Lucana *et al.*, 2004) and a comparative sequence analysis (Fig. 1) shows that HbpS shares a high homology with proteins of unknown function from the Gram-positive bacteria *S. coelicolor* (Bentley *et al.*, 2002), *Rhodococcus* sp. RHA1 (McLeod *et al.*, 2006), *Arthrobacter aurescens* TC1 (Mongodin *et al.*, 2006) as well as the pathogenic Gram-negative bacteria *Vibrio cholera* (Heidelberg *et al.*, 2000) and *Klebsiella pneumoniae* (Arakawa *et al.*, 1995).

The production of HbpS is greatly increased *in vivo* during the cultivation of *S. reticuli* and *S. lividans* transformants in the presence of the naturally occurring antibiotic haemin and HbpS has been shown directly to bind haemin (Ortiz de Orué Lucana *et al.*, 2004). Haemin, a natural porphyrin, is known to possess significant antibacterial activity when augmented by physiological concentrations of hydrogen peroxide or reducing agents (Stojiljkovic *et al.*, 2001; Baker *et al.*, 2003); it has therefore been suggested that HbpS-like proteins may play an important role in defence against haemin-based toxicity (Ortiz de Orué Lucana *et al.*, 2004). Studies have also demonstrated that secretion of HbpS is carried out under the control of the twin-arginine translocation (TAT) pathway, through which folded and oligomeric proteins are translocated across the outer cell membrane (Chaddock *et al.*, 1995; Berks, 1996). The native oligomeric state of HbpS is currently unclear as SDS–PAGE analysis of wild-type secreted HbpS indicates the presence of monomeric, dimeric and higher order oligomers (Ortiz de Orué Lucana *et al.*, 2004).

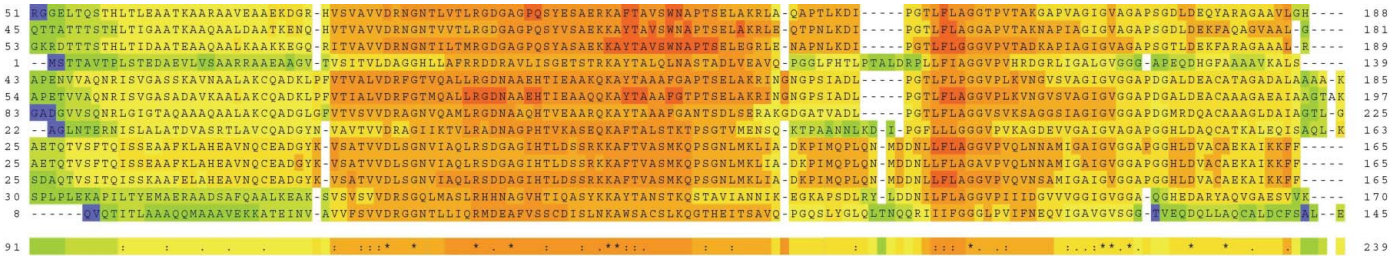

Figure 1
A sequence alignment of HbpS-like proteins colour-coded by sequence conservation (blue, lowest; red, highest). The predicted signal peptides (where appropriate) have been removed to improve the quality of the alignment. The following symbols are used in the 'conserved' alignment displayed at the bottom of the figure: '.' weakly conserved, ':' strongly conserved, '*' absolutely conserved. This figure was generated from the sequence alignment performed by the package *T-COFFEE* (Notredame *et al.*, 2000).

The disruption of HbpS also induces a significant decrease in the *in vivo* production of CpeB, a mycelia-associated haem-containing enzyme (Zou *et al.*, 1999). CpeB has been shown to utilize H_2O_2 to oxidize a number of substrates *via* an attached haem group (ferric protoporphyrin) or in a haem-independent reaction, which is coupled to manganese(II)/(III) peroxidation (Zou & Schrempf, 2000). As the haem-dependent catalase activity of CpeB leads to the dissociation of H_2O_2 to H_2O and O_2, it also plays an important part in the detoxification of H_2O_2.

CpeB shows a high degree of amino-acid identity (62% identity, 73% similarity) to the catalase–peroxidase KatG from *Mycobacterium tuberculosis*. The front-line anti-tuberculosis drug isoniazid (isonicotinic acid hydrazide) requires KatG activation before exerting a lethal effect (Zhang *et al.*, 1992) and isoiazid-resistant strains of *M. tuberculosis* have been shown to possess no detectable levels of KatG, although they acquire a compensatory mutation resulting in an upregulation of expression of an alkyl hydroperoxide reductase protein, AhpC (Sherman *et al.*, 1996). Sherman and coworkers suggested that KatG would confer protection against H_2O_2-mediated damage, even in the absence of adequate catalase and peroxidase activities, thus promoting survival of the organism in the environment of the phagocyte oxidative burst.

A specific interaction has been identified between HbpS and the sensor kinase SenS from the recently identified two-component sensor system, SenS–SenR, which negatively regulates the *furS–cpeB* operon and the *hbpS* gene (Ortiz de Orué Lucana *et al.*, 2005; Bogel *et al.*, 2007). Disruption of the SenS–SenR two-component system also results in an increased sensitivity of *S. reticuli* to haemin and hydrogen peroxide. The closest available annotated homologue of SenS is the sensor kinase ChrS of *Corynebacterium diphtheriae* (34% identity, 46% similarity), which has been shown to play a role in the utilization of haem and haemoglobin as iron sources (Schmitt, 1999).

This homology in HbpS and HbpS interaction partners implies a common functional role across a wide range of bacterial species, including a number of medically relevant bacteria. From the previous research reviewed above, the major role of HbpS-like proteins would appear to be the regulation of the expression of CpeB/KatG-like proteins in response to extracellular redox conditions (*i.e.* the presence of H_2O_2, haemin *etc*.) that are detrimental to bacterial survival. In order to gain further insight into the physiological role of HbpS-like proteins, we have overexpressed recombinant wild-type HbpS from *S. reticuli* in *Escherichia coli* for examination and in this report we detail the crystallization and X-ray diffraction characterization of the crystals obtained. The measurement of experimental phases, using a brief halide soak, is described and the current status of the three-dimensional model is given.

2. Materials and methods

2.1. Cleavage of DNA, ligation and agarose gel electrophoresis

The DNAs were cleaved with various restriction enzymes according to the suppliers' instructions. Ligation was performed with T4 ligase (Promega). Gel electrophoresis was carried out in 0.8–2% agarose gels using Tris–borate–EDTA (TBE) buffer (89 m*M* Tris, 89 m*M* boric acid and 2 m*M* EDTA pH 8.0). *E. coli* was transformed with plasmid DNA by electroporation (Dower *et al.*, 1988). Plasmids were isolated from *E. coli* with the aid of a mini plasmid kit (Qiagen).

2.2. Cloning of the *hbpS* gene into an *E. coli* expression plasmid

The *hbpS*-coding region (without the codons encoding for the signal peptide) was amplified by PCR from the previously described construct pWKS10 (Zou *et al.*, 1999) using the primers HBP8 (5′-GAGA**CCATGG**CCGACACCACGGAG-3′), consisting of an *Nco*I restriction site (bold) followed by the sequence encoding the N-terminal amino acids of the mature HbpS (without the signal peptide), and HBP9 (5′-GGGC**AAGCTT**GTGGCCGAGCACGG-3′) coding for the C-terminal amino acids of HbpS followed by the *Hin*dIII restriction site (bold). The PCR product was digested with

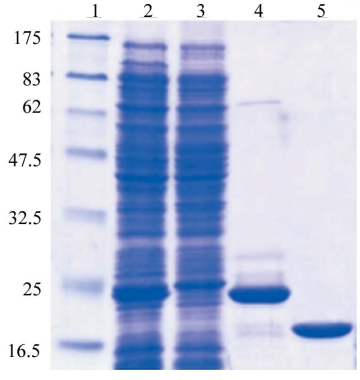

Figure 2
An SDS–PAGE analysis of the purified HbpS. The *E. coli* BL21 (DE3) pLysS strain containing the plasmid pETHbpS was grown and induced as described in §2. The cytoplasmic fraction containing His_6-tag-HbpS (lane 2) was incubated with Ni-NTA agarose. Unbound proteins remained in the flowthrough (lane 3). His_6-tag-HbpS was eluted in the presence of 250 m*M* imidazole (lane 4). The His_6 tag was then cleaved using TEV-protease; after a second Ni-NTA affinity chromatography, HbpS was then further purified by anion-exchange chromatography through DEAE-Sepharose (lane 5). The molecular weight (in kDa) of each of the protein markers is indicated (lane 1). A total of 5 mg purified His_6-tag-free HbpS was obtained from 1 l of bacterial culture.

*Nco*I and *Hin*dIII, ligated with *Nco*I/*Hin*dIII-cleaved pETM11 and subsequently transformed into *E. coli* XL1-blue. Sequencing of the resulting plasmid (pETHbpS) confirmed the presence of the *hbpS* gene in frame fusion with the His_6 tag and the TEV-protease cleavage site.

2.3. Production and purification of HbpS

The plasmid pETHbpS was transformed into *E. coli* strain BL21 (DE3) pLysS. Protein expression was induced at OD_{600} = 0.6 at 310 K with 1 m*M* IPTG for 4 h. Cell pellets were resuspended in buffer *W* (150 m*M* NaCl, 20 m*M* Tris–HCl pH 8) containing DNaseI (1 µg ml^{-1}) and then lysed by ultrasonication (Branson sonifier, 5 × 10 s, with 10 s intervals). After centrifugation, the supernatant was incubated with Ni-NTA agarose (Qiagen) in the presence of an additional 25 m*M* imidazole. The resin was washed with buffer *W* and the protein was then eluted with buffer *W* containing an additional 250 m*M* imidazole. The eluted protein was incubated overnight in the presence of 5 m*M* DTT and His_6-tag-TEV protease for cleavage of the His_6 tag. Imidazole and DTT were removed from the protein solution using PD10 columns (Amersham) previously equilibrated in buffer *W*. A second Ni-NTA affinity chromatography was performed to remove remaining His_6 tags, His_6-tagged TEV protease and uncleaved His_6-tag-HbpS. The solution containing unbound proteins (His_6-tag-free HbpS) was then desalted into buffer *A* (20 m*M* Tris–HCl pH 7) using PD10 columns (Amersham). HbpS was then further purified by anion-exchange chromatography over a DEAE-Sepharose column previously equilibrated in 20 m*M* Tris–HCl pH 7. Interestingly, under such conditions HbpS (pI 5.9) does not interact with the matrix and remains in the flowthrough in high purity (over 99% as judged from SDS–PAGE analysis; Fig. 2). The protein sequence was confirmed by mass-spectrometric analysis (ESI LC-MS) and the protein was concentrated to 14 mg ml^{-1} for crystallization, as judged from its absorbance at 280 nm (ε_o = 8250 cm^{-1} M^{-1}; MW = 15 498 Da).

3. Results and discussion

3.1. Crystallization of HbpS

Purified HbpS was submitted to the high-throughput crystallization facility at the EMBL Hamburg (Mueller-Dieckmann, 2006) at the concentration described above. Sitting-drop sizes were 200 + 200 nl, equilibrated over 50 µl screen reagent. A large number of conditions (32 of 576 conditions screened) resulted in crystals and were screened for diffraction properties on beamline X13, EMBL-Hamburg. After initial diffraction screening, the crystals grown from the cryocondition sparse-matrix screen [40%(*v*/*v*) PEG 400, 100 m*M* MES pH 6.0, 5%(*w*/*v*) PEG 3000; Emerald Biostructures Wizard Cryo Screens I and II; deCODE Biostructures] were identified as those providing the highest initial diffraction quality. Subsequently, manual hanging-drop optimization screens were performed around these conditions, varying buffer pH and PEG concentrations, in order to reproduce and improve the crystal size. Optimized crystals exhibited pyramidal morphology and grew to maximum dimensions of 200 × 150 × 150 µm (Fig. 3). Final optimized conditions were in the range 39–42%(*v*/*v*) PEG 400, 100 m*M* MES pH 5.8–6.5, 5%(*v*/*v*) PEG 3000. Owing to the components of the crystallization experiment, no further cryoprotection was required for diffraction experiments at 100 K.

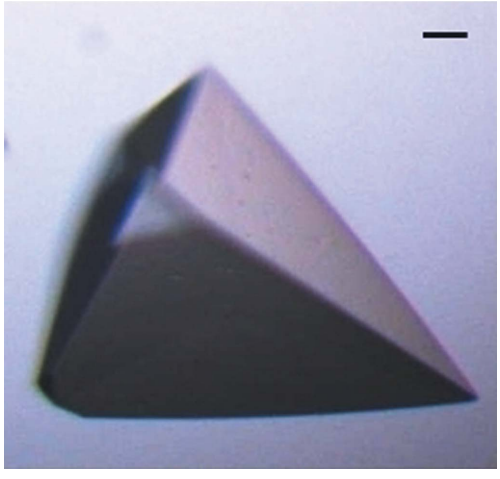

Figure 3
An image of a typical HbpS crystal grown as described in §3.1. The bar in the upper right corner corresponds to 10 µm.

3.2. Diffraction experiments using native HbpS crystals

A native data set was collected from optimized HbpS crystals on beamline BW7A, EMBL-Hamburg, in dose mode. The collection of initial frames was performed to allow crystal characterization and space-group assignment using the software *POINTLESS* (Evans, 2006). Subsequently, the data-collection strategy software *BEST* (Popov & Bourenkov, 2003) was used to design a data-collection experiment suitable for the time available on the beamline which would provide a signal-to-noise ratio of over 3 at the edge of the detector used (Fig. 4; MarCCD-165 mm). A 2.2 Å native data set was collected, with statistics as detailed in Table 1. Data were processed

Figure 4
A typical diffraction image obtained from the HbpS native crystals. This image was collected on beamline BW7A, EMBL-Hamburg, under cryoconditions (100 K) from a single crystal mounted directly from the crystallization conditions described. Exposure times were approximately 300 s, dependent upon the storage-ring intensity, for an oscillation range of 0.2°. The incident wavelength was 0.98 Å and the resolution at the edge of the detector was 2.2 Å. Further details of the data-collection parameters are given in Table 1.

Table 1
Data-collection parameters for the native and sodium-bromide-soaked crystals of HbpS.

Values in parentheses refer to the high-resolution shell of the respective data set.

	Native HbpS	15 s soak in 1 *M* NaBr
Experimental conditions		
Beamline	BW7A (EMBL Hamburg)	X12 (EMBL-Hamburg)
Wavelength (Å)	0.9778	0.9197
Temperature (K)	100	100
Detector	Mar-CCD 165 mm	Mar-CCD 225 mm
Crystal parameters		
Space group	$P2_13$	$P2_13$
Unit-cell parameters (Å, °)	$a = b = c = 152.5$, $\alpha = \beta = \gamma = 90$	$a = b = c = 151.9$, $\alpha = \beta = \gamma = 90$
Data-collection parameters		
Resolution range (Å)	20–2.20 (2.40–2.20)	20–3.4 (3.7–3.4)
Mosaicity (°)	0.18	0.33
Crystal-to-detector distance (mm)	174	295
Oscillation range (°)	0.2	0.3
No. of frames	450	140
Data-processing parameters		
No. of measured reflections	247495 (59161)	70896 (10638)
No. of unique reflections	37888 (12979)	29023 (5005)
Multiplicity	6.53 (4.56)	2.44 (2.12)
Completeness (%)	98.5 (94.9)	93.2 (76.1)
$I/\sigma(I)$	12.63 (3.56)	9.77 (3.87)
$R_{\rm merge}$† (%)	7.3 (32.1)	9.2 (26.5)
$R_{\rm meas}$‡ (%)	8.1 (38.6)	11.4 (33.5)
Mean anomalous difference§	n/a	1.127 (0.854)

† Merging R factor, $R_{\rm merge} = \sum_{hkl}\sum_i |I_i(hkl) - \langle I(hkl)\rangle| / \sum_{hkl}\sum_i I_i(hkl)$. ‡ Redundancy-independent R factor, $R_{\rm meas} = \sum_{hkl}[N/(N-1)]^{1/2}\sum_i |I_i(hkl) - \langle I(hkl)\rangle| / \sum_{hkl}\sum_i I_i(hkl)$ (Diederichs & Karplus, 1997). § Mean anomalous difference in units of its estimated standard deviation $[|F(+) - F(-)|/\sigma]$. $F(+)$, $F(-)$ are structure-factor estimates obtained from the merged intensity observations in each parity class.

using *XDS* and merged in *XSCALE* (Kabsch, 1988). A sequence search of the Protein Data Bank (Berman *et al.*, 2000) using *BLAST* (Altschul *et al.*, 1990) revealed that no structures of significant sequence homology were available for use as molecular-replacement models, requiring the collection of experimental phases. Native HbpS crystals were briefly soaked (15 s) in the crystallization well solution containing an additional 1 *M* sodium bromide (Dauter *et al.*, 2000). Immediately following the soaking experiments, the crystals were mounted on beamline X12, EMBL-Hamburg, and screened for diffraction. The data-collection strategy software *BEST* (Popov & Bourenkov, 2003) was again used to design an SAD data-collection experiment which would provide a signal-to-noise ratio of 4 at the edge of the detector used (MarCCD-225 mm). A 3.4 Å data set was collected at a wavelength above the bromine edge (0.9197 Å), with statistics as detailed in Table 1. As described above for the native data, derivative data were processed using *XDS* and merged in *XSCALE* (Kabsch, 1988). The solvent content (Matthews, 1968) was predicted for a number of different oligomeric states, with between six and eight molecules predicted to occupy the asymmetric unit.

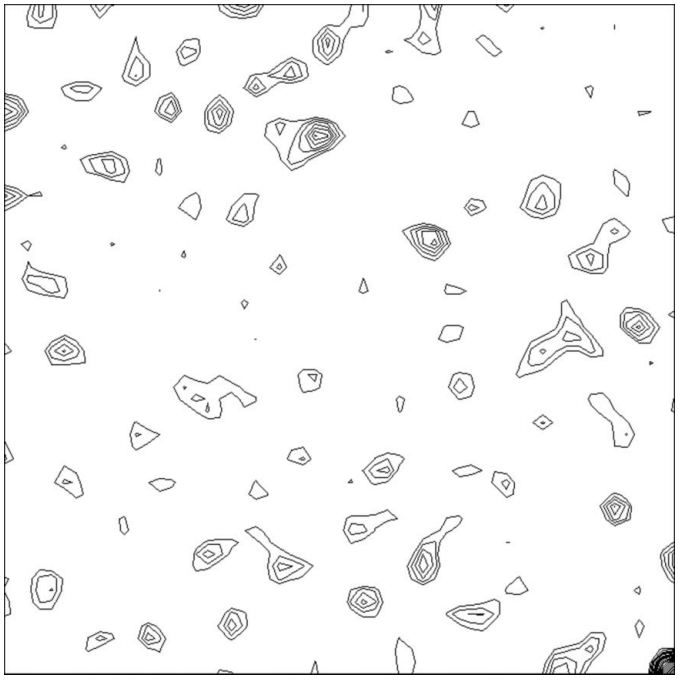

Figure 5
An anomalous Patterson map from data collected on the sodium-bromide-soaked crystals. The map corresponds to the Harker section ($Z = 1/2$) of the space group $P2_13$. The map is contoured from 1σ in 0.5σ steps. Signals originating from multiple bound bromine ions can be distinguished. 20 individual bromide ions were finally used in the phasing protocol of *SOLVE* (Terwilliger & Berendzen, 1999). See §3.3 for further details.

3.3. Phase determination

Initial analysis of the anomalous signal from the bromide-soaked crystals indicated the presence of bound bromine ions, with significant peaks available in the Harker sections of the anomalous Patterson maps (Fig. 5). Subsequently, the package *SOLVE* (Terwilliger & Berendzen, 1999) was used to identify 20 independent bromine sites with an overall figure of merit of 0.21. Refinement of the experimental phases and automated building of the sequence into the resulting electron-density maps were performed using *RESOLVE* (Terwilliger, 2000, 2003). The initial figure of merit of phasing was 0.42 and the final figure of merit after automated building of 777 amino-acid residues was 0.60. Examination of the resulting electron-density maps indicated that HbpS is present as an octomer in the asymmetric unit, indicating that approximately 62% of the structure (777 out of 1248 residues) was built by *RESOLVE*. Further model building and refinement of the full structure are currently in progress.

The authors acknowledge the support of EMBL-Hamburg, in particular that of the scientists responsible for the beamlines BW7A

(Dr Andrea Schmidt) and X12 (Dr Manfred S. Weiss). We thank Professor Dr Hildgund Schrempf for stimulating discussions. This work was also supported in part by grant OR 224/1-1 of the Deutsche Forschungsgemeinschaft (DFG).

References

Altschul, S. F., Gish, W., Miller, W., Myers, E. W. & Lipman, D. J. (1990). *J. Mol. Biol.* **215**, 403–410.
Arakawa, Y., Wacharotayankun, R., Nagatsuka, T., Ito, H., Kato, N. & Ohta, M. (1995). *J. Bacteriol.* **177**, 1788–1796.
Baker, H. M., Anderson, B. F. & Baker, E. N. (2003). *Proc. Natl Acad. Sci. USA*, **100**, 3579–3583.
Bentley, S. D. *et al.* (2002). *Nature (London)*, **417**, 141–147.
Berks, B. C. (1996). *Mol. Microbiol.* **22**, 393–404.
Berman, H. M., Westbrook, J., Feng, Z., Gilliland, G., Bhat, T. N., Weissig, H., Shindyalov, I. N. & Bourne, P. E. (2000). *Nucleic Acids Res.* **28**, 235–242.
Bogel, G., Schrempf, H. & Ortiz de Orué Lucana, D. (2007). *FEBS J.* **274**, 3900–3913.
Chaddock, A. M., Mant, A., Karnauchov, I., Brink, S., Herrmann, R. G., Klösgen, R. B. & Robinson, C. (1995). *EMBO J.* **14**, 2715–2722.
Dauter, Z., Dauter, M. & Rajashankar, K. R. (2000). *Acta Cryst.* D**56**, 232–237.
Diederichs, K. & Karplus, P. A. (1997). *Nature Struct. Biol.* **4**, 269–275.
Dower, W. J., Miller, J. F. & Ragsdale, C. W. (1988). *Nucleic Acids Res.* **16**, 6127–6145.
Evans, P. (2006). *Acta Cryst.* D**62**, 72–82.
Heidelberg, J. F. *et al.* (2000). *Nature (London)*, **406**, 477–483.
Kabsch, W. (1988). *J. Appl. Cryst.* **21**, 916–924.
McLeod, M. P. *et al.* (2006). *Proc. Natl Acad. Sci. USA*, **103**, 15582–15587.
Matthews, B. W. (1968). *J. Mol. Biol.* **33**, 491–497.
Mongodin, E. F. *et al.* (2006). *PloS Genet.* **2**, e214.
Mueller-Dieckmann, J. (2006). *Acta Cryst.* D**62**, 1446–1452.
Notredame, C., Higgins, D. & Heringa, J. (2000). *J. Mol. Biol.* **302**, 205–217.
Ortiz de Orué Lucana, D., Schaa, T. & Schrempf, H. (2004). *Microbiology*, **150**, 2575–2585.
Ortiz de Orué Lucana, D., Zou, P., Nierhaus, M. & Schrempf, H. (2005). *Microbiology*, **151**, 3603–3614.
Popov, A. N. & Bourenkov, G. P. (2003). *Acta Cryst.* D**59**, 1145–1153.
Schmitt, M. P. (1999). *J. Bacteriol.* **181**, 5330–5340.
Sherman, D. R., Mdluli, K., Hickey, M. J., Arain, T. M., Morris, S. L., Barry III, C. E. & Stover, C. K. (1996). *Science*, **272**, 1641–1643.
Stojiljkovic, I., Evavold, B. D. & Kumar, V. (2001). *Expert Opin. Investig. Drugs*, **10**, 309–320.
Terwilliger, T. C. (2000). *Acta Cryst.* D**56**, 965–972.
Terwilliger, T. C. (2003). *Acta Cryst.* D**59**, 38–44.
Terwilliger, T. C. & Berendzen, J. (1999). *Acta Cryst.* D**55**, 849–861.
Zhang, Y., Heym, B., Allen, B., Young, D. & Cole, S. (1992). *Nature (London)*, **358**, 591–593.
Zou, P., Borovok, I., Ortiz de Orué Lucana, D., Muller, D. & Schrempf, H. (1999). *Microbiology*, **145**, 549–559.
Zou, P. & Schrempf, H. (2000). *Eur. J. Biochem.* **267**, 2840–2849.